Journal of Colloid and Interface Science 597 (2021) 314–324

Contents lists available at ScienceDirect

Journal of Colloid and Interface Science

journal homepage: www.elsevier.com/locate/jcis

Regular Article

Discrimination of dopamine by an electrode modified with negatively charged manganese dioxide nanoparticles decorated on a poly(3,4 ethylenedioxythiophene)/reduced graphene oxide composite

Kiattisak Promsuwan [a,b,c], Asamee Soleh [a,b,c], Kasrin Saisahas [e], Jenjira Saichanapan [d], Proespichaya Kanatharana [a,b,c], Panote Thavarungkul [a,b,c], Chunxian Guo [h], Chang Ming Li [f,g,h,*], Warakorn Limbut [a,b,d,*]

[a] Center of Excellence for Trace Analysis and Biosensor, Prince of Songkla University, Hat Yai, Songkhla 90112, Thailand
[b] Center of Excellence for Innovation in Chemistry, Faculty of Science, Prince of Songkla University, HatYai, Songkhla 90112, Thailand
[c] Division of Physical Science, Faculty of Science, Prince of Songkla University, Hat Yai, Songkhla 90112, Thailand
[d] Division of Health and Applied Sciences, Faculty of Science, Prince of Songkla University, Hat Yai, Songkhla 90112, Thailand
[e] Forensic Science Programme, School of Health Sciences, Universiti Sains Malaysia, 16150 Kubang Kerian, Kelantan, Malaysia
[f] School of Chemical and Biomedical Engineering, Nanyang Technological University, 637457, Singapore
[g] Institute for Clean Energy & Advanced Materials, Faculty of Materials and Energy, Southwest University, Chongqing 400715, PR China
[h] Institute of Materials Science & Devices, Suzhou University of Science and Technology, Suzhou 215011, PR China

GRAPHICAL ABSTRACT

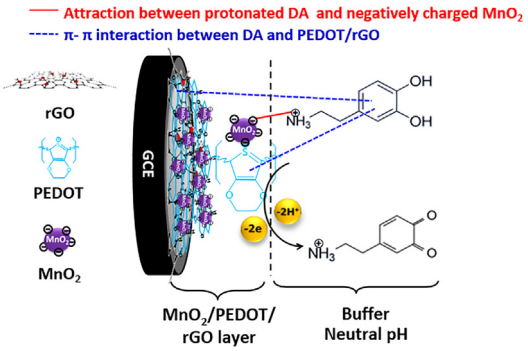

ARTICLE INFO

Article history:
Received 12 February 2021
Revised 26 March 2021
Accepted 27 March 2021
Available online 31 March 2021

Keywords:
Negatively charged manganese dioxide nanoparticles
Poly(3,4-ethylenedioxythiophene)
Reduced graphene oxide
Dopamine

ABSTRACT

A unique nanocomposite was fabricated using negatively charged manganese dioxide nanoparticles, poly (3,4-ethylenedioxythiophene) and reduced graphene oxide (MnO_2/PEDOT/rGO). The nanocomposite was deposited on a glassy carbon electrode (GCE) functionalized with amino groups. The modified GCE was used to electrochemically detect dopamine (DA). The surface morphology, charge effect and electrochemical behaviours of the modified GCE were characterized by scanning electron microscopy, energy dispersive X-ray analysis (EDX), cyclic voltammetry and electrochemical impedance spectroscopy, respectively. The MnO_2/PEDOT/rGO/GCE exhibited excellent performance towards DA sensing with a linear range between 0.05 and 135 μM with a lowest detection limit of 30 nM (S/N = 3). Selectivity towards DA was high in the presence of high concentrations of the typical interferences ascorbic acid and uric acid. The stability and reproducibility of the electrode were good. The sensor accurately determined DA in human serum. The synergic effect of the multiple components of the fabricated nanocomposite were critical to the good DA sensing performance. rGO provided a conductive backbone, PEDOT directed the

* Corresponding authors.
E-mail addresses: cxguo@usts.edu.cn (C. Guo), ecmli@usts.edu.cn (C.M. Li), WARAKORN.L@PSU.AC.TH (W. Limbut), WARAKORN.L@PSU.AC.TH (W. Limbut).

https://doi.org/10.1016/j.jcis.2021.03.162

uniform growth of MnO_2 and adsorbed DA via pi-pi and electrostatic interaction, while the negatively charged MnO_2 provided adsorption and catalytic sites for protonated DA. This work produced a promising biosensor that sensitively and selectively detected DA.

1. Introduction

Dopamine (DA) is a crucial neurotransmitter, playing a significant role in the functioning of the central nervous, renal, hormonal, and cardiovascular systems [1–3]. An abnormal level of DA in extracellular fluid often leads to neurological disorders such as schizophrenia, Huntington's disease, and Parkinson's disease [1,4]. In the past few years, several approaches to the determination of DA have been developed, including colorimetry [5], fluorometry [6,7], chemiluminescence [8], capillary electrophoresis [9] and electrochemical sensing [10–12]. Among these approaches, electrochemical sensing has advantages of high sensitivity, rapid response, simple operation, and ease of miniaturization [13,14]. However, the concentration of DA in human body fluids is low. The normal physiological level of DA is between 10^{-5} and 10^{-3} mM [15,16]. High concentrations of ascorbic acid (AA) and uric acid (UA) in bodily fluids can interfere significantly with results since they are easily oxidized at a potential close to the oxidization potential of DA [17,18]. Therefore, when developing a material-based sensor to determine DA, a major challenge is the discrimination of DA from coexisting AA and UA in human body fluids. In the past decade, several modified electrode surfaces have been designed and fabricated to separate oxidation peaks of DA, AA, and UA. The modifying materials used have included conducting polymers [19,20], carbon nanomaterials [21,22], metal/metal oxide nanoparticles [23], and their composites [13,24]. Since DA is positively charged (pK_a = 8.9) in normal physiological conditions, whereas ascorbic acid (pK_a = 4.2) and uric acid (pK_a = 5.7) are negatively charged, their oxidation peaks can be separated by negatively charging the electrode interface to attract the cationic DA and repel the anionic AA and UA [25,26]. One of the conducting polymers widely used to modify electrodes for application in electrochemical DA sensors is poly(3,4-ethylenedioxythiophene) (PEDOT) [26,27]. PEDOT has a high inherent conductivity, a broad electrochemical window, good chemical stability and is easy to modulate [26–28]. Moreover, it can be doped with negatively charged molecules. In electrochemical DA detection sensors, it has been applied in composites as PEDOT/SDS [29], PEDOT-PANS [30], PEDOT:Nafion [31], PEDOT:PSS [32], and PEDOT:Citrate [26]. However, these negatively charged molecules also have some limitations since they only generate negative charges on the interface and not electro-catalytic properties.

Metal oxide nanoparticles have shown some advantages in electrochemical analysis because they not only exhibit unique electro-catalytic performances [33], but their surfaces can also be negatively charged [34,35]. Among metal oxide nanoparticles, manganese dioxide (MnO_2) nanoparticles are also commonly used for catalysis and electrochemical sensor applications because they possess good catalytic properties, high specific capacitance, are non-toxic and, compared to nickel oxide, ruthenium oxide, cobalt oxide, and cerium oxide, low-cost [36–38]. There are many reports of DA sensors that integrated electrodes modified with MnO_2 combined with carbon materials (multi-walled carbon nanotubes and graphene) which showed high electrocatalytic oxidation of DA [37,39]. The properties of PEDOT can be tailored with MnO_2 nanoparticles decorated on the PEDOT interface. The decoration is a facile procedure performed by letting MnO_2 nanoparticles directly grow on PEDOT via a redox exchange of $KMnO_4$ precursor with the sulfur sites on PEDOT structures [36,38]. The negatively charged MnO_2 nanoparticles on the PEDOT surface can enhance the electrochemical detection of DA because PEDOT can interact with DA molecules via hydrophobic interaction, and the negative surface charges on MnO_2 nanoparticles can accumulate the positively charged DA before electro-catalysis. These properties of MnO_2 nanoparticles and PEDOT could be used as a selective component for a DA detection transducer.

Another important factor of electrode modification is the efficiency of conductivity and the electro-active surface area of the composite electrode. In the past decade, the introduction of two-dimensional (2D) carbon materialsd, especially, graphene (Gr) has received great attention in electrochemical sensor applications. The highly delocalized π-conjugation system of Gr endows the material with excellent electrical conductivity and a large specific surface area, which accelerated interfacial electron transfer [36,37,40,41]. For this reason, graphene is frequently applied as an electrode component to increase electrode conductivity and surface area.

We herein report a facile approach to the direct fabrication of a unique nanocomposite comprising negatively charged MnO_2 nanoparticles decorated on poly(3,4-ethylenedioxythiophene) (PEDOT) and supported by chemically reduced graphene oxide on a glassy carbon electrode (GCE) (MnO_2/PEDOT/rGO/GCE) and its application in sensitive and selective DA detection. The fabrication process was schematically presented in Scheme 1. The morphology of the nanocomposite was characterized using scanning electron microscopy (SEM), and energy dispersive x-ray analysis (EDX). The electrochemical behaviors, the surface charge effect of each nanocomposite, and electrode kinetics were proved by cyclic voltammetry (CV) and electrochemical impedance spectroscopy. The performance of the nanocomposite-based sensor towards DA oxidation detection was investigated and compared with the performances of control samples including the MnO_2/rGO/GCE, PEDOT/rGO/GCE, rGO/GCE and the bare GCE. The reproducibility, stability, and long-term stability of the proposed sensor were tested. The accuracy of the MnO_2/PEDOT/rGO/GCE sensor was evaluated by determination of spiked DA in real human serum.

2. Experimental

2.1. Chemical and reagents

Potassium permanganate ($KMnO_4$, Sigma-Aldrich), 3-aminopropyl triethoxysilane (APTES, $C_9H_{23}NO_3Si$, Sigma-Aldrich), ascorbic acid ($C_6H_8O_6$, Aldrich), 3,4-ethylenedioxythiophene (EDOT, $C_6H_6O_2S$, Aldrich), lithium perchlorate trihydrate ($LiClO_4 \cdot 3H_2O$, Aldrich), DA hydrochloride ($C_8H_{11}NO_2 \cdot HCl$, Sigma), uric acid ($C_5H_4N_4O_3$, Sigma), and graphite powder (purum, Fluka) were reagent grade quality and used without further purification. All other chemicals were analytical grade and obtained from Sigma-Aldrich. All solutions were prepared using deionized (18 MΩ·cm) from a Milli-Q water purifier. Phosphate buffer solution (PB, 0.1 M, pH 6.60) was prepared from K_2HPO_4 and KH_2PO_4. Solutions of DA, AA, and UA were freshly prepared before use.

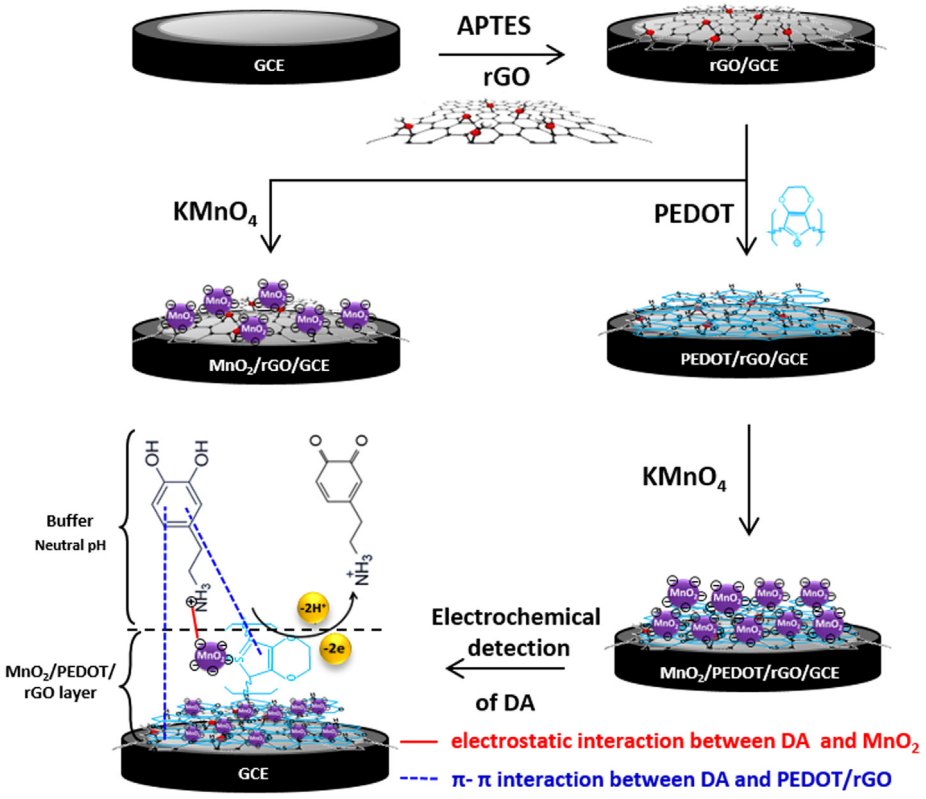

Scheme 1. Fabrication procedure of the rGO/GCE, PEDOT/rGO/GCE, MnO_2/rGO/GCE, and MnO_2/PEDOT/rGO/GCE. The inset shows the proposed mechanism of DA detection.

2.2. Synthesis of reduced graphene oxide (rGO)

GO was synthesized by oxidation of natural graphite powder according to a reported modified Hummers method using $NaNO_3$, H_2SO_4, and $KMnO_4$ [42]. The oxidized material was purified by washing with 10% (V/V) HCl solution, repeatedly rinsing with copious amounts of Milli-Q water, and vacuum filtering. GO was obtained by dissolving the as-prepared oxidized material in distilled water to a concentration of 0.2 mg ml^{-1}, followed by sonication under ambient conditions for 60 min. The solution was then centrifuged. The above GO solution was converted to rGO by hydrazine reduction.

2.3. Fabrication of MnO_2/PEDOT/rGO/GCE

The fabrication process of the MnO_2/PEDOT/rGO/GCE was schematically presented in Scheme 1. The GCE was polished to a mirror finish with light pressure following a figure-8 pattern using 1, 0.3 and 0.05 μm alumina slurries. The polished electrode was sonicated in deionized water and dried in a nitrogen stream. The rGO modified GCE was fabricated as previously reported [43]. The polished GCE surface was activated using cyclic voltammetry in 0.05 M H_2SO_4 scanning for 10 cycles from 0 to 2000 mV versus an Ag/AgCl reference electrode at a scan rate of 50 mV s^{-1}. The activated electrode was then washed with copious amounts of deionized water and dried in a nitrogen stream. The activated GCE was then modified with aminopropyltriethoxysilane (APTES), which acted as a cross-linker between GCE and rGO. The activated GCE was immersed in 1% APTES anhydrous toluene solution for 15 h, thoroughly rinsed with anhydrous toluene and dried in a nitrogen stream. In this step, APTES molecules were assembled on the activated GCE surface via the C—O—Si bond. The APTES modified GCE was immersed in 0.1 mg ml^{-1} rGO for 4 h, to let rGO form siloxane bonds (–Si–O–Si–) with APTES-GCE, thereby leading to the covering of rGO on GCE to obtain rGO/GCE. The rGO/GCE was covered with PEDOT film by electrochemical polymerization in 0.1 M H_2SO_4 containing 0.01 M EDOT and 0.2 M $LiClO_4$ using ten scans of CV in a potential range from 200 to 1200 mV versus an Ag/AgCl reference electrode at a scan rate of 50 mV s^{-1}. The PEDOT/rGO/GCE was then washed with copious amounts of deionized water and dried in a nitrogen stream. MnO_2 nanoparticles were decorated on the PEDOT/rGO/GCE by immersing the PEDOT/rGO/GCE in 10 mM $KMnO_4$ for 10 min [38]. MnO_2 nanoparticles directly grew on PEDOT via a redox exchange of $KMnO_4$ with the sulfur sites on the PEDOT structure [36,38]. The electrode was thoroughly rinsed with deionized water and dried with a stream of nitrogen. A control sample of MnO_2 nanoparticles was decorated on the rGO/GCE via the intercalation and adsorption of manganese ions onto rGO, followed by the nucleation and growth of MnO_2 as previously reported [44].

2.4. Apparatus and electrochemical measurements

The morphology of samples was investigated by field emission scanning microscopy (SEM, JSM-6700F, Japan). Cyclic voltammetry (CV), linear sweep voltammetry (LSV) and amperometric measurements were performed using an Autolab model PGSTAT30 (Metrohm-EcoChemie) controlled by a personal computer using GPES software version 4.9 from. All the electrochemical measurements were carried out using a conventional three-electrode system with an Ag/AgCl reference electrode and a platinum wire auxiliary electrode. The surface charge effect of each nanocomposite was evaluated using CV in 0.1 M KCl containing both positively charged and negatively charged redox probes. The electrochemical behaviours of DA, AA and UA were characterized by CV in 0.1 M PB (pH 6.60) by applying potential from −200 to 800 mV at a scan rate

of 50 mV s^{-1} versus an Ag/AgCl reference electrode. LSV was used to check interference effects from AA and UA in DA detection, which was carried out in 0.1 M PB by applying potential from −200 to 800 V versus an Ag/AgCl reference electrode with sweep scan of 50 mV s^{-1}. Amperometric measurement of DA in spiked human serum samples was performed in 0.1 M PB (pH 6.60) by applying a constant potential of 195 V versus an Ag/AgCl reference electrode. For all electrochemical measurements, a few microliters of standard DA, AA and UA solutions were injected with a micropipette into an electrochemical cell filled with 5 mL of PB and the current due to direct oxidation of the analyte was measured. All experiments were performed at room temperature.

3. Results and discussion

3.1. Morphology characterization

The morphology of samples was characterized by SEM. The bare GCE had quite a rough surface (Fig. 1**A**). The rGO/GCE showed a layer of thin film with clearly observed wrinkles (Fig. 1**B**). Wrinkles are a common characteristic of graphene sheets deposited on flat surfaces [17]. The electrodeposition of PEDOT produced a uniform film composed of ultra-small nanoparticles (~10 nm) (Fig. 1**D**), indicating a good interaction between PEDOT and graphene, which might be from the π-π interaction between the six-atom ring of the PEDOT molecule and the six-carbon ring of graphene. After the growth of MnO_2 on the PEDOT/rGO/GCE, nanospheres were formed as seen in the low magnification SEM image (Fig. 1**E**). Under high magnification SEM image (Fig. 1**F**), it can be seen that the nanospheres were uniformly nanoscale with a size around 50 nm. MnO_2 nanoparticles were also grown directly on rGO via the intercalation and adsorption of manganese ions without the use of PEDOT, followed by the nucleation and growth of MnO_2 nanoparticles on the rGO surface [44]. The resulting structure was compact and non-uniform (Fig. 1**C**). These results demonstrated that PEDOT played an important role in the uniform growth of MnO_2 nanoparticles on the rGO surface. It was suggested recently that MnO_2 can also be directly grown on PEDOT via a redox reaction [36,38]. Thus, for the uniform deposition of MnO_2, PEDOT might not only provide anchoring sites to promote the initial nucleation but also be an

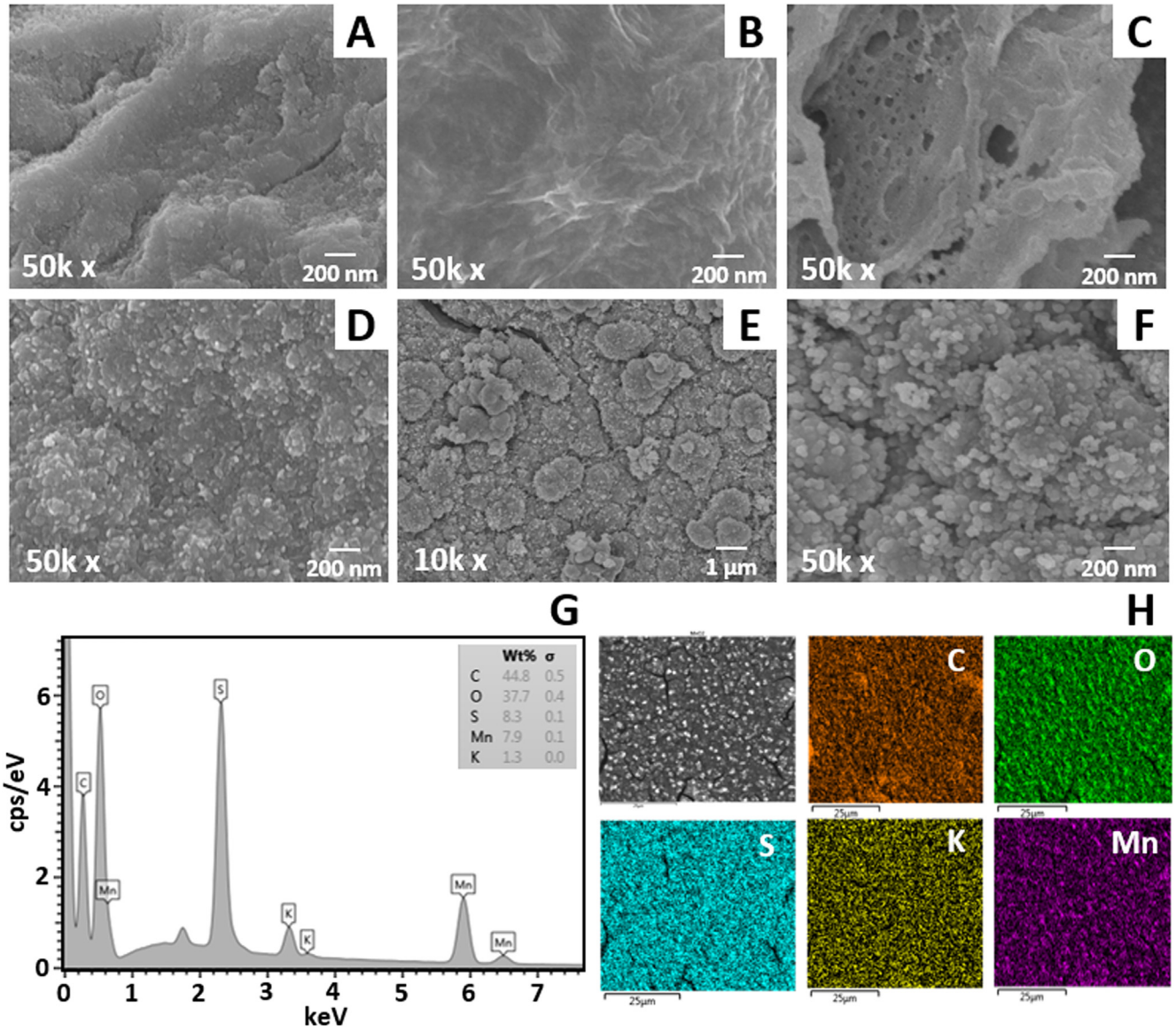

Fig. 1. SEM images of surfaces of the GCE (A), rGO/GCE (B), MnO_2/rGO/GCE (C), PEDOT/rGO/GCE (D) at 50,000× magnification and MnO_2/PEDOT/rGO/GCE at 10,000× magnification (E) and 50,000× (F). (G) EDX spectrum and (H) EDX mapping of the MnO_2/PEDOT/rGO compoite.

active agent to grow MnO_2. EDX measurement from area analysis of the MnO_2/PEDOT/rGO electrode showed the presence of C, O, S, Mn, and K at percentages of about 44.8%, 37.7%, 8.3%, 7.9%, and 1.3%, respectively **(**Fig. 1**G)**. This was an important indication of the formation of MnO_2/PEDOT/rGO nanocomposites on the electrode surface. EDX mapping of MnO_2/PEDOT/rGO revealed a uniform distribution of carbon, oxygen, sulfur, potassium, and manganese (Fig. 1**H**), which was indicative of the successful coupling of rGO, PEDOT and MnO_2.

3.2. Surface charge characterization

To prove the surface charge effect of modified electrode, a positively charged $Ru(NH_3)_6^{2+/3+}$ redox probe and a negatively charged $Fe(CN)_6^{3-/4-}$ redox probe were applied. In the positively charged $Ru(NH_3)_6^{2+/3+}$ system (Fig. 2**A**), the bare GCE (curve a) produced a pair of redox peaks. At the rGO/GCE (curve b) the redox peak of the probe increased due to the larger background charge currents, indicating the enhanced conductivity of the electroactive surface area of the electrode. At the MnO_2/rGO/GCE (curve c), the background charge current was similar to the current at the rGO/GCE, but the redox peaks of the $Ru(NH_3)_6^{2+/3+}$ were higher. This was due to the surface charge effect of the negatively charged MnO_2. The background charge currents dramatically increased at the PEDOT/rGO/GCE (curve d) and the redox peaks of the probe were no longer present. This was probably due to the positively charged surface of PEDOT [26,28] which repelled the $Ru(NH_3)_6^{2+/3+}$ probe. Furthermore, at the MnO_2/PEDOT/rGO/GCE (curve e), the redox peak of $Ru(NH_3)_6^{2+/3+}$ probe reappeared. This result indicated that the positively charged $Ru(NH_3)_6^{2+/3+}$ probe was electrostatically attracted to the electrode surface by the negatively charged MnO_2 nanoparticles [45–47].

In the negatively charged $Fe(CN)_6^{3-/4-}$ probe system (Fig. 2**B**), a pair of reversible redox peaks were produced at the bare GCE (curve a), while at the rGO/GCE (curve b), the redox peak of the probe was clearly increased by comparison with the bare GCE. This was attributed to the excellent electronic conductivity of rGO and the large surface area of its wrinkled structure [17]. The redox peak clearly decreased at the MnO_2/rGO/GCE (curve c). This was probably due to the negatively charged surface of MnO_2 [35,48], which repelled the $Fe(CN)_6^{3-/4-}$ probe. At the PEDOT/rGO/GCE (curve d), the background charge current sharply increased with the increased redox current of the $Fe(CN)_6^{3-/4-}$ probe. This was probably due to the high energy storage capacity, good electrical conductivity and the positive charge in the PEDOT backbone, which attracted the $Fe(CN)_6^{3-/4-}$ probe to the electrode surface [28]. On the other hand, at the MnO_2/PEDOT/rGO/GCE (curve d), the background charge currents decreased, and the redox peak current decreased dramatically. This suggested that the negatively charged probe did not reach the negatively charged surface of the MnO_2/PEDOT/rGO/GCE due to electrostatic repulsion [46,47,49]. Moreover, to evaluate the electroactive surface area of the different modified electrodes, CV information of Fig. 2B can be applied to calculate the electroactive surface area via the Randle-Sevcik equation ($I_{p,a} = 2.69 \times 10^5\ n^{3/2} A C D^{1/2}\ \nu^{1/2}$). The electroactive surface area of 0.054, 0.071, 0.063, 0.082, and 0.100 cm^2 were calculated for the bare GCE, rGO/GCE, MnO_2/rGO/GCE, PEDOT/rGO/GCE and MnO_2/PEDOT/rGO/GCE, respectively.

To further evaluate the electrochemical properties of individual materials present in the nanocomposite, EIS was carried out in a

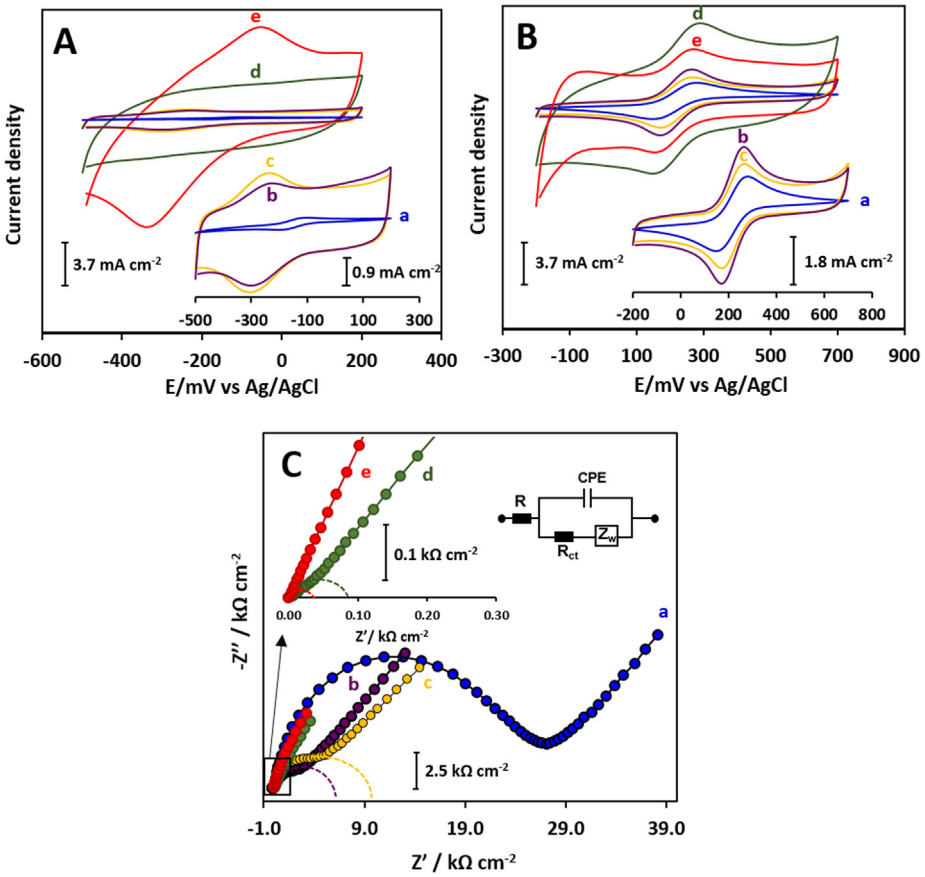

Fig. 2. CVs of 0.1 M KCl containing 5.0 mM $Ru(NH_3)_6^{2+/3+}$ (A) and 5.0 mM $Fe(CN)_6^{3-/4-}$ (B) on bare GCE (a), rGO/GCE (b), MnO_2/rGO/GCE (c) PEDOT/rGO/GCE (d) and MnO_2/PEDOT/rGO/GCE (d) at a scan rate of 50 mV s^{-1}. (C) Nyquist plots fitted with equivalent electrical circuit (inset).

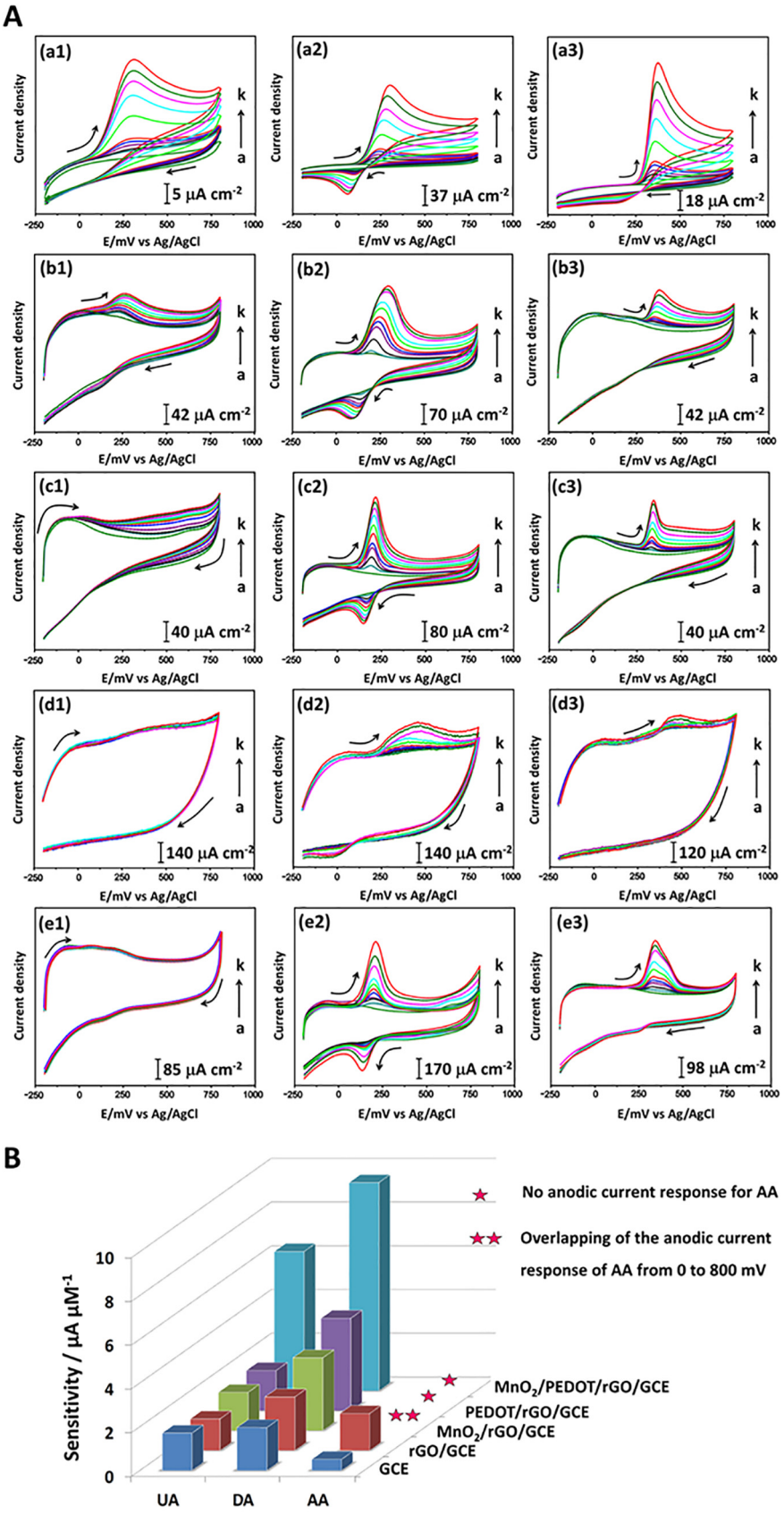

Fig. 3. **(A)** CVs of different electrodes in different concentrations (a → k: 0, 10, 20, 30, 40, 50, 98, 146, 192, 238, 283 μM) of AA (**1**), DA (**2**) and UA (**3**): on the GCE (**a1**), (**a2**) and (**a3**); on the rGO/GCE (**b1**), (**b2**) and (**b3**); on the MnO_2/rGO/GCE (**c1**), (**c2**) and (**c3**); on the PEDOT/rGO/GCE (**d1**), (**d2**) and (**d3**); on the MnO_2/PEDOT/rGO/GCE (**e1**), (**e2**) and (**e3**). **(B)** The chart compares the sensitivity of detection (slope of calibration curve) toward AA, DA and UA of the different modified electrodes.

5.0 mM $Fe(CN)_6^{3-/4-}$ containing 0.1 M KCl solution, and the corresponding Nyquist plots are presented in Fig. 2C. All the Nyquist plots for each modified electrode material composed of a semicircle in the high-frequency region corresponding to the charge transfer process with the semicircle diameter equivalent to the charge transfer resistance (R_{ct}) and a linear part at a low frequency relating to the diffusion process. These Nyquist plots were well fitted with equivalent Randles circuit (Fig. 2C (inset), Compared to the bare GCE (curve a) (27.4 kΩ cm^{-2}), the R_{ct} values of the rGO/GCE (curve b) showed smaller (7.3 kΩ cm^{-2}), indicating that the rGO/GCE promotes electron transfer and improves the conductivity of the surface of the electrode. While the MnO_2/rGO/GCE (curve c), the R_{ct} value was increased to 10.7 kΩ cm^{-2}, this may be attributed to the repulsion of the negatively charged redox probe by the negatively charged surface of MnO_2. At the PEDOT/rGO/GCE (curve e), the R_{ct} value dramatically decreased to 0.04 kΩ cm^{-2}, indicating a good electrical conductivity with a positive charge of the PEDOT/rGO/GCE. In contrast, when presents MnO_2 on PEDOT/rGO/GCE (curve d), the R_{ct} value was increased slightly (0.08 kΩ cm^{-2}), suggesting that the negatively charged surface of the MnO_2 on PEDOT/rGO/GCE repel the negatively charged probe owing to electrostatic repulsion effect.

3.3. Electrochemical behaviors of AA, DA, and UA at different modified electrodes

The electrochemical behaviors of different electrodes were studied by comparing the cyclic CVs and sensitivity toward AA, DA and UA at different concentrations (10–283 μM) at the bare GCE, rGO/GCE, MnO_2/rGO/GCE, PEDOT/rGO/GCE, and MnO_2/PEDOT/rGO/GCE. CVs of responses at the bare GCE exhibited a broad anodic potential peak for AA, DA, and UA at 283, 252, and 357 mV, respectively, with relatively low response (Fig. 3**A** (**a1**), (**a2**) and (**a2**)). Compared to the GCE, the anodic peak potentials of AA at the rGO/GCE (Fig. 3**A (b1)**), DA (Fig. 3**A (b2)**), and UA (Fig. 3**A (b3)**) appeared nearly the same, but the anodic current peak and sensitivity of DA (Fig. 3**B**) were higher possibly due to π-π interaction between rGO and DA molecules [21,50]. In addition, the anodic peaks of AA, DA and UA at the GCE and rGO/GCE overlapped. These results indicated that rGO increased the response toward DA, but its selectivity was still poor. In the case of the MnO_2/rGO/GCE, the anodic peaks of DA (Fig. 3**A (c2)**) and UA (Fig. 3**A (c3)**) were separated by 110 mV and sensitivity was increased (Fig. 3**B**), which was very likely the result of the attraction of positively charged DA molecules to negatively charged MnO_2 nanoparticles prior to electrocatalysis (Scheme 1). However, the anodic peak response of AA still overlapped with that of DA from 0 to 800 mV (Fig. 3**A (c1)**). For the PEDOT/rGO/GCE, the anodic response and sensitivity of DA were enhanced compared with the rGO/GCE (Fig. 3**A (d2)** and Fig. 3**B**), which might have been due to the hydrophobic interaction between DA and PEDOT [51] (Scheme 1). The interference of AA was also eliminated (Fig. 3**A (d1)**), which can be explained as follows. At neutral pH, the anion of AA cannot react through electrostatic interaction with PEDOT/rGO due to counter-ion charge balancing between the positive charge of PEDOT and the negative charge of rGO. On the other hand, the anodic peak of DA on PEDOT/rGO/GCE was still broad and overlapped the peak of UA (Fig. 3**A (d3)**). The interference of AA was eliminated at the MnO_2/PEDOT/rGO/GCE and peak potentials of DA and UA were around 140 mV apart (Fig. 3**A (e1), (e2)) and (e3)**). In addition, sensitivity toward DA was highest on the MnO_2/PEDOT/rGO/GCE, possibly due to the synergetic effect of MnO_2 and PEDOT, which could react via hydrophobic interaction. Also, the uniform distribution of negatively charged MnO_2 nanoparticles could efficiently accumulate the positively charged DA molecules to its surface prior to electro-catalytic oxidation of DA to DA o-quinone, as shown in Scheme 1.

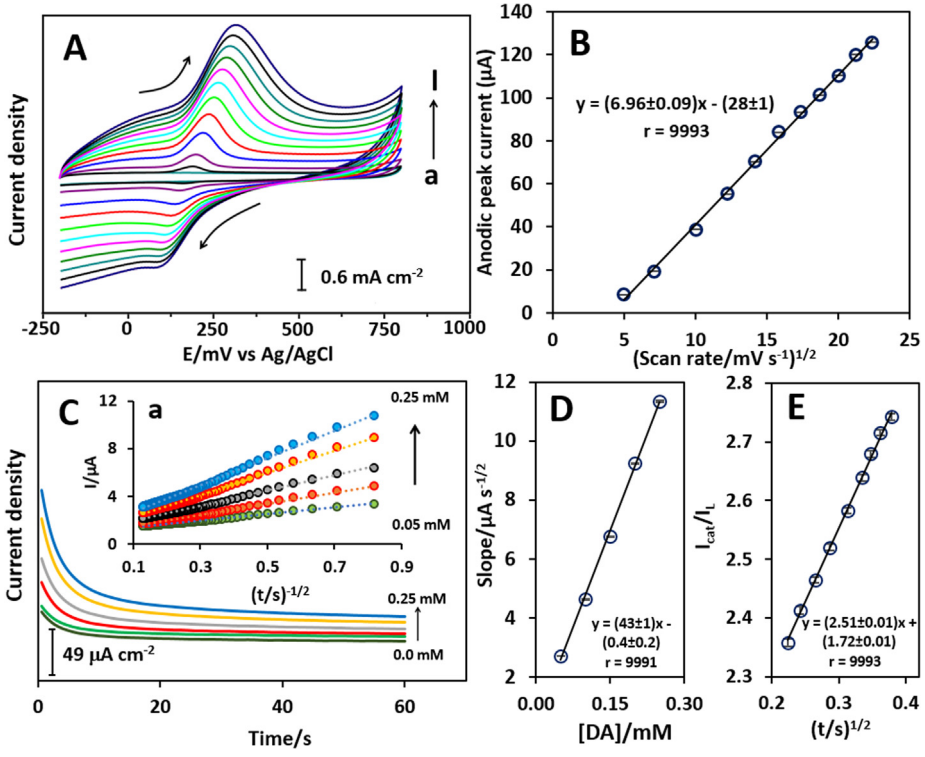

Fig. 4. (A) CVs of MnO_2/PEDOT/rGO/GCE at different scan rates (a → l; 25 to 500 mV s^{-1}) in PB at pH 6.60 containing 100 μM DA. (B) The plot between anodic peak current versus the square root of the scan rate. (C) Chronoamperograms of MnO_2/PEDOT/rGO/GCE at different concentrations of DA. (D) the slope of the plot of I versus $t^{-1/2}$ and DA concentrations and (E) the plot of I_{cat}/I_L vs $t^{1/2}$.

3.4. Scan rate and electro-kinetics of DA at MnO_2/PEDOT/rGO/GCE

The electrochemical oxidation behavior of DA on the MnO_2/PEDOT/rGO/GCE was investigated. Both the anodic current peak and cathodic current peak were affected by the scan rate. The redox peak currents gradually increased as the scan rate was increased (Fig. 4**A**). The calibration curve of anodic peak current versus the square root of the scan rate over a range from 25 to 500 mV s^{-1} showed a good linear relationship (Fig. 4**B**). The linear regression equation was I_{ac} (μA) = 6.96 × (ν/mv s^{-1})$^{1/2}$ –28.54, with a correlation coefficient of 0.9993. The good linear relationship indicated that the electrochemical oxidation of DA on MnO_2/PEDOT/rGO/GCE was a diffusion-controlled process.

To evaluate the diffusion coefficient in the diffusion-limited electrocatalytic process of DA oxidation on the MnO_2/PEDOT/rGO/GCE, a series concentration of DA (0.05, 0.10, 0.15, 0.20, and 0.25 mM) was measured in PB (pH 6.60) by chronoamperometry at 195 mV. Cottrell's equation (1) was applied to calculate the diffusion coefficient (D):

$$I = nFAD^{1/2} C_b \pi^{-1/2} t^{-1/2} \quad (1)$$

where D, C_b, F, n, and A, respectively, refer to the diffusion coefficient of the analyte (cm^2 s^{-1}), analyte bulk concentration (mol cm^{-3}), the Faraday constant, the numbers of electrons, and the electrode geometric area. Linear curves of I versus $t^{-1/2}$ were plotted from the raw chronoamperometric data for different concentrations of DA (Fig. 4**C (a)**). Based on the straight-line slope between DA concentrations and the slope of the plot of I versus $t^{-1/2}$ (Fig. 4**D**), the diffusion coefficient of DA on MnO_2/PEDOT/rGO/GCE was calculated to be (3.28 ± 0.05) × 10^{-5} cm^2 s^{-1}. Moreover, to quantify of the catalytic contribution of MnO_2 on PEDOT/rGO/GCE to DA was investigated via the catalytic rate constant (k_{cat}) value using the chronoamperometric data (Fig. 4C). Therefore, the k_{cat} value for the reaction between DA and the MnO_2/PEDOT/rGO/GCE was calculated based on Galus using equation ($I_{Cat}/I_L = \pi^{1/2} \gamma^{1/2} = \pi^{1/2} (k_{cat}C_b t)^{1/2}$)[52], where I_{Cat} and I_L respectively, are the currents measured in the presence and absence of DA, kcat is the catalytic rate constant (mol^{-1} L s^{-1}), C is the bulk concentration (M) and t

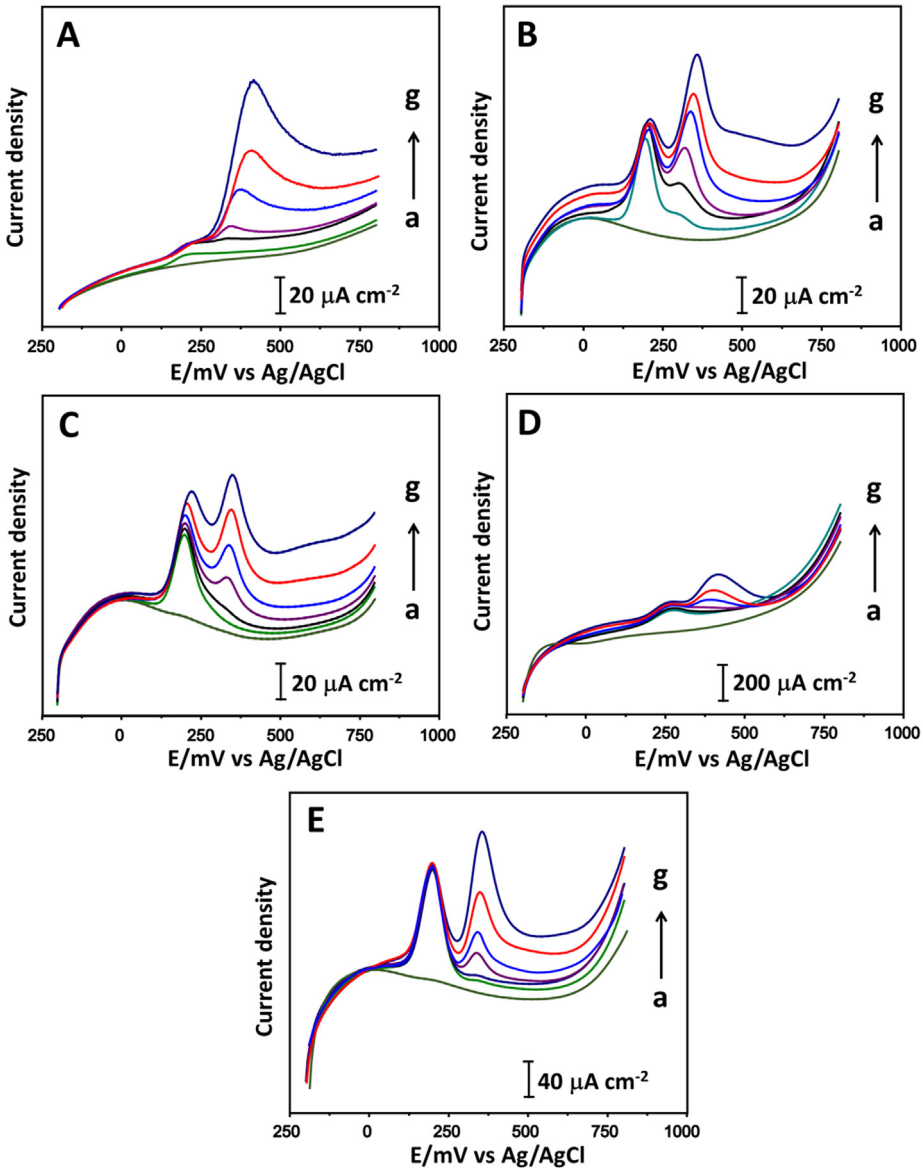

Fig. 5. LSVs of the GCE (A), rGO/GCE (B), MnO_2/rGO/GCE (C), PEDOT/rGO/GCE (D), and MnO_2/PEDOT/rGO/GCE (E) at different concentration ratios of AA:DA:UA (a → g; 0:0:0 (blank), 0:10:0, 2.5:10:2.5, 25:10:25, 125:10:125, 250:10:250, 500:10:500 μM).

is time (s) elapsed. From the slope of I_{Cat}/I_L vs. $t^{1/2}$ (Fig. 4E), the k_{cat} value was calculated to be (2.01 ± 0.05) × 10^4 mol^{-1} L s^{-1}.

3.5. Interference study

Interference effects were studied in detail from linear sweep voltammograms (LSVs) with different ratios of AA:DA:UA (0:0:0 (blank), 0:10:0, 2.5:10:2.5, 25:10:25, 125:10:125, 250:10:250, 500:10:500 μM) (Fig. 5). The GCE (Fig. 5**A**), rGO/GCE (Fig. 5**B**), and MnO_2/rGO/GCE (Fig. 5**C**) all exhibited serious overlapping in the voltammograms of both AA and UA to DA. In addition, when the concentration of DA was kept constant at 10 μM, the anodic peak current increased with increments of AA and DA concentration from 2.5 to 500 μM (Fig. 5**A, B, and C; c to g**). These results indicated the poor selectivity of the GCE, rGO/GCE and MnO_2/rGO/GCE towards both AA and DA. The PEDOT/rGO/GCE (Fig. 5**D**) did not give any response towards AA. However, its anodic peak responses towards DA and UA could not be differentiated. Moreover, its anodic peak currents towards DA increased with increments of UA concentration (Fig. 5**D; c to g**), indicating poor selectivity towards UA. In contrast, the MnO_2/PEDOT/rGO/GCE (Fig. 5**E**) exhibited an excellent selectivity for DA detection and effectively eliminated the AA interference while differentiating the anodic peak of DA and UA. In addition, the anodic peak of DA on the MnO_2/PEDOT/rGO/GCE remained constant even in higher concentrations of AA and UA up to 500 μM (Fig. 5**E; c to g**) The MnO_2/PEDOT/rGO/GCE demonstrated excellent selectivity toward DA.

3.6. Amperometric DA detection using MnO_2/PEDOT/rGO/GCE

Fig. 6**A** shows the calibration curves of the anodic current from amperometric measurement versus the concentration of DA at the MnO_2/PEDOT/rGO/GCE and the PEDOT/rGO/GCE. The MnO_2/PEDOT/rGO/GCE exhibited a linear range from 0.05 to 135 μM with a linear regression equation of I (anodic current, 10^{-6} A cm^{-2}) = (0.247 ± 0.002) × DA concentration (μM) + (0.45 ± 0.09) and a correlation coefficient of 0.999. In addition, the detection limit of the MnO_2/PEDOT/rGO/GCE was 30 nM (at a signal-to-noise ratio of 3). Fig. 6**B** presents the amperometric response of the MnO_2/PEDOT/rGO/GCE to successive additions of various concentrations of DA, AA and UA. The anodic current response toward DA reached about 95% of the steady-state current within 8 s while no anodic

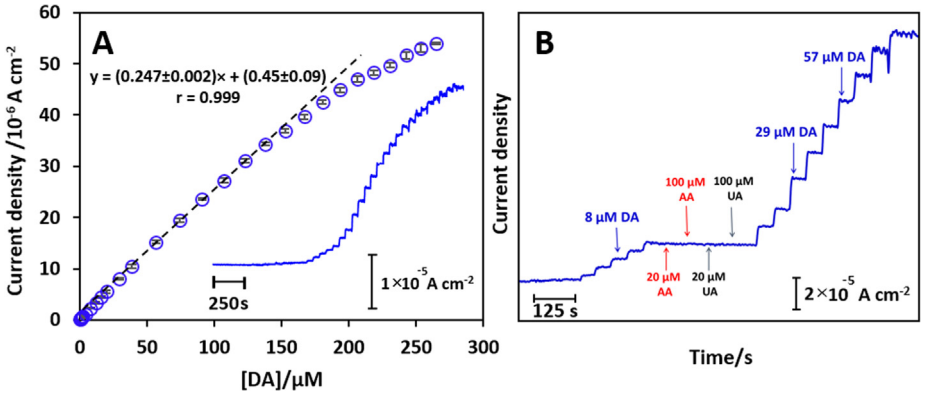

Fig. 6. (A) The linear relationships between anodic current and DA concentration of the MnO_2/PEDOT/rGO/GCE Inset: Current-time response of MnO_2/PEDOT/rGO/GCE at 195 mV to successive additions of various concentrations of DA in 0.1 M PB (pH 6.60). (B) Current-time response of MnO_2/PEDOT/rGO/GCE at 195 mV to successive additions of various concentrations of DA, AA, and UA in 0.1 M PB (pH 6.60).

Table 1
Comparison of analytical performances in the determination of DA at various PEDOT-based composite modified electrodes.

Electrode	Technique	Linear range/μM	LOD/μM	Ref.
Citrate:PEDOT/GCE	DPV	1–85	0.15	[26]
CD/NF/PEDOT/Au	DPV	2–320	0.003	[53]
SDS/PEDOT/Pt	LSV	0.5–25, 30–100	0.061	[29]
Ionic liquid/PEDOT /GCE	Amperometry	0.2–312	0.051	[54]
PEDOT/CNT/CPE	DPV	0.1–20	0.02	[55]
Pd/PEDOT/GCE	DPV	0.5–1	0.5	[56]
NiO/PEDOT/CNT/ GCE	DPV	0.03–20	0.026	[24]
CeO_2/PEDOT/MWCNTs/GCE	DPV	0.10–10 and 40–400	0.03	[13]
MnO_2/PEDOT/rGO/GCE	Amperometry	0.05–135	0.03	This work

Table 2
Recovery of DA from human serum samples (n = 5).

Human Serum	Spike(μM)	Found(μM)	%RSD(n = 5)	%Recovery(n = 5)
1	2.0	1.90 ± 0.06	3.1	97 ± 3
2	4.0	3.8 ± 0.1	3.0	95 ± 3
3	5.0	4.90 ± 0.09	1.9	98 ± 2
4	6.0	6.10 ± 0.05	0.9	102 ± 1
5	8.0	8.3 ± 0.1	1.4	104 ± 1
6	10.0	9.6 ± 0.2	2.4	96 ± 2

current responses were produced for the interfering species of AA and UA.

The analytical performances of the MnO_2/PEDOT/rGO/GCE toward DA were compared with those from other reported works that used electrodes modified with PEDOT-based composites (Table 1). Compared with other PEDOT-based electrodes, the proposed MnO_2/PEDOT/rGO/GCE exhibited good performances with respect to both the linear detection range and the limit of detection. However, our MnO_2/PEDOT/rGO/GCE also had some limitations in terms of the lengthy multi-step fabrication process.

3.7. Reproducibility and stability

The reproducibility of the preparation of the MnO_2/PEDOT/rGO/GCE was tested by checking the sensitivity (slope) of five electrodes. The mean value of sensitivity was 0.03 $\mu A\ \mu M^{-1}$ and the relative standard deviation (RSD) was 3.3%. These results indicated the good reproducibility of the preparation process. The response reproducibility of the electrode towards oxidation of DA was analyzed from 30 measurements of the amperometric response in 0.1 M PB pH 6.60 containing 2 μM DA. The RSD was as low as 2.7%, confirming the very good response reproducibility. The long-term stability of the proposed modified electrode was evaluated by measuring the sensitivity for six weeks storage at room temperature. The sensitivity of the MnO_2/PEDOT/rGO/GCE retained more than 83% of the initial value, which is reasonably good.

3.8. Real sample analysis

To evaluate the practical application of the MnO_2PEDOT/rGO/GCE for DA detection, human serum samples were selected for analysis. The accuracy and recovery tests were conducted by preparing human serum samples spiked with defined DA concentrations. The spiked samples were then injected directly into 5.0 mL 0.1 M PB (pH 6.60) without any pretreatment. The responses from six spiked samples were summarized in Table 2. The percentage recoveries of DA in human serum samples were in the range of 95 ± 3 to 104 ± 1% with RSDs between 0.9 and 3.1%. These results demonstrated that the MnO_2-PEDOT/rGO/GCE is a practical means of DA detection in real biological samples.

4. Conclusions

We reported a unique nanocomposite of manganese dioxide nanoparticles (MnO_2), poly (3,4-ethylenedioxythiophene) (PEDOT) and reduced graphene oxide (rGO) on a glassy carbon electrode (GCE) and the excellent performane of the modified electrode towards DA detection. PEDOT played bi-functional roles in the uniform distribution of MnO_2, as a provider of anchoring sites to promote the initial nucleation and as an active agent to grow MnO_2 with a negative charge. The results reveal that each component in the nanocomposite played an important role in DA sensing. rGO provided the conductive sites and increased the surface area of the electrode, PEDOT directed the uniform growth of MnO_2 and adsorbed DA via hydrophobic interaction while MnO_2 with its negatively charged surface attracted the positively charged DA. The MnO_2/PEDOT/rGO/GCE provides the sensitivity higher than 5.26-fold, 3.77-fold, 2.85-fold, and 2.23-fold for the controls of the bare GCE, rGO/GCE, MnO_2/rGO/GCE, and PEDOT/rGO/GCE. The developed electrode effectively eliminated interference from high concentrations of ascorbic acid and uric acid. In addition, the MnO_2/PEDOT/rGO/GCE exhibited a low detection limit (30 nM), and good reproducibility and stability. The electrode accurately determined DA in human serum. The excellent analytical performances of the MnO_2/PEDOT/rGO/GCE make this electrode a promising platform for sensitive and selective DA detection. Further development of miniaturized microelectrode systems would be possible by integrating the nanocomposite with a carbon-fiber microelectrode to monitor neuronal activity in the brain by DA detection. In addition, this alternative MnO_2/PEDOT/rGO/ electrode composite can be useful and pave to possible application in other fields such as biosensors, biofuel cells, and supercapacitors in the future.

Declaration of Competing Interest

The authors declare that they have no known competing financial interests or personal relationships that could have appeared to influence the work reported in this paper.

Acknowledgment

This work was supported by Prince of Songkla University (grant no. SCI540110N) and the Thailand Research Fund (TRF) and Prince of Songkla University (grant no. RSA 6280081). The Center of Excellence for Innovation in Chemistry (PERCH-CIC), Ministry of Higher Education, Science, Research and Innovation, the Center of Excellence for Trace Analysis and Biosensor (TAB-CoE) and the Graduate School and Faculty of Science, Prince of Songkla University, Hat Yai, Thailand, and the School of Chemical and Biomedical Engineering, Nanyang Technological University are gratefully acknowledged. Thanks also to Mr Thomas Duncan Coyne, Faculty of Science, Prince of Songkla University, Hat Yai, Songkhla, Thailand for assistance with the English text.

References

[1] R.M. Wightman, L.J. May, A.C. Michael, Detection of dopamine dynamics in the brain, Anal. Chem. 60 (1988) 769A–779A.
[2] A. Zhang, J.L. Neumeyer, R.J. Baldessarini, Recent Progress in Development of Dopamine Receptor Subtype-Selective Agents: Potential Therapeutics for Neurological and Psychiatric Disorders, Chem. Rev. 107 (2007) 274–302.
[3] M.F. Lokhandwala, R.J. Barrett, Cardiovascular dopamine receptors: physiological, pharmacological and therapeutic implications, J. Auton. Pharmacol. 2 (1982) 189–215.
[4] J.J. Weinstein, M.O. Chohan, M. Slifstein, L.S. Kegeles, H. Moore, A. Abi-Dargham, Pathway-Specific Dopamine Abnormalities in Schizophrenia, Biol. Psychiatry 81 (2017) 31–42.
[5] H. Liu, Y.-N. Ding, B. Bian, L. Li, R. Li, X. Zhang, Z. Liu, X. Zhang, G. Fan, Q. Liu, Rapid colorimetric determination of dopamine based on the inhibition of the peroxidase mimicking activity of platinum loaded CoSn(OH)6 nanocubes, Microchim. Acta 186 (2019) 755.
[6] Y. Suzuki, Design and synthesis of fluorescent reagents for selective detection of dopamine, Sens. Actuators, B 239 (2017) 383–389.
[7] J. Yang, Z. Zeng, J. Kang, S. Betzler, C. Czarnik, X. Zhang, C. Ophus, C. Yu, K. Bustillo, M. Pan, J. Qiu, L.-W. Wang, H. Zheng, Formation of two-dimensional transition metal oxide nanosheets with nanoparticles as intermediates, Nat. Mater. 18 (2019) 970–976.
[8] W. Gao, L. Qi, Z. Liu, S. Majeed, S.A. Kitte, G. Xu, Efficient lucigenin/thiourea dioxide chemiluminescence system and its application for selective and sensitive dopamine detection, Sens. Actuators, B 238 (2017) 468–472.
[9] A. Roychoudhury, K.A. Francis, J. Patel, S.K. Jha, S. Basu, A decoupler-free simple paper microchip capillary electrophoresis device for simultaneous detection of dopamine, epinephrine and serotonin, RSC Adv. 10 (2020) 25487–25495.
[10] S.K. Arumugasamy, S. Govindaraju, K. Yun, Electrochemical sensor for detecting dopamine using graphene quantum dots incorporated with multiwall carbon nanotubes, Appl. Surf. Sci. 508 (2020) 145294.
[11] Y. Yang, M. Li, Z. Zhu, A novel electrochemical sensor based on carbon nanotubes array for selective detection of dopamine or uric acid, Talanta 201 (2019) 295–300.
[12] S. Yang, J. Zhao, S. Tricard, L. Yu, J. Fang, A sensitive and selective electrochemical sensor based on N, P-Doped molybdenum Carbide@Carbon/Prussian blue/graphite felt composite electrode for the detection of dopamine, Anal. Chim. Acta 1094 (2020) 80–89.
[13] A. Üğe, D. Koyuncu Zeybek, B. Zeybek, An electrochemical sensor for sensitive detection of dopamine based on MWCNTs/CeO2-PEDOT composite, J. Electroanal. Chem. 813 (2018) 134–142.
[14] I.M. Taylor, E.M. Robbins, K.A. Catt, P.A. Cody, C.L. Happe, X.T. Cui, Enhanced dopamine detection sensitivity by PEDOT/graphene oxide coating on in vivo carbon fiber electrodes, Biosens. Bioelectron. 89 (2017) 400–410.

[15] J. Kim, M. Jeon, K.-J. Paeng, I.R. Paeng, Competitive enzyme-linked immunosorbent assay for the determination of catecholamine, dopamine in serum, Anal. Chim. Acta 619 (2008) 87–93.
[16] T. Jiang, G. Jiang, Q. Huang, H. Zhou, High-sensitive detection of dopamine using graphitic carbon nitride by electrochemical method, Mater. Res. Bull. 74 (2016) 271–277.
[17] X. Chen, D. Li, W. Ma, T. Yang, Y. Zhang, D. Zhang, Preparation of a glassy carbon electrode modified with reduced graphene oxide and overoxidized electropolymerized polypyrrole, and its application to the determination of dopamine in the presence of ascorbic acid and uric acid, Microchim. Acta 186 (2019) 407.
[18] Y. Li, H. Lin, H. Peng, R. Qi, C. Luo, A glassy carbon electrode modified with MoS2 nanosheets and poly(3,4-ethylenedioxythiophene) for simultaneous electrochemical detection of ascorbic acid, dopamine and uric acid, Microchim. Acta 183 (2016) 2517–2523.
[19] S.S. Kumar, J. Mathiyarasu, K.L.N. Phani, V. Yegnaraman, Simultaneous determination of dopamine and ascorbic acid on poly (3,4-ethylenedioxythiophene) modified glassy carbon electrode, J. Solid State Electrochem. 10 (2006) 905–913.
[20] L. Sasso, A. Heiskanen, F. Diazzi, M. Dimaki, J. Castillo-León, M. Vergani, E. Landini, R. Raiteri, G. Ferrari, M. Carminati, M. Sampietro, W.E. Svendsen, J. Emnéus, Doped overoxidized polypyrrole microelectrodes as sensors for the detection of dopamine released from cell populations, Analyst 138 (2013) 3651–3659.
[21] Y. Wang, Y. Li, L. Tang, J. Lu, J. Li, Application of graphene-modified electrode for selective detection of dopamine, Electrochem. Commun. 11 (2009) 889–892.
[22] H. Bi, Y. Li, S. Liu, P. Guo, Z. Wei, C. Lv, J. Zhang, X.S. Zhao, Carbon-nanotube-modified glassy carbon electrode for simultaneous determination of dopamine, ascorbic acid and uric acid: The effect of functional groups, Sens. Actuators, B 171–172 (2012) 1132–1140.
[23] O.E. Fayemi, A.S. Adekunle, B.E. Kumara Swamy, E.E. Ebenso, Electrochemical sensor for the detection of dopamine in real samples using polyaniline/NiO, ZnO, and Fe3O4 nanocomposites on glassy carbon electrode, J. Electroanal. Chem. 818 (2018) 236–249.
[24] D. Sun, H. Li, M. Li, C. Li, H. Dai, D. Sun, B. Yang, Electrodeposition synthesis of a NiO/CNT/PEDOT composite for simultaneous detection of dopamine, serotonin, and tryptophan, Sens. Actuators, B 259 (2018) 433–442.
[25] A. Liu, M.D. Wei, I. Honma, H. Zhou, Biosensing Properties of TitanateNanotube Films: Selective Detection of Dopamine in the Presence of Ascorbate and Uric Acid, Adv. Funct. Mater. 16 (2006) 371–376.
[26] L. Meng, A.P.F. Turner, W.C. Mak, Modulating Electrode Kinetics for Discrimination of Dopamine by a PEDOT:COOH Interface Doped with Negatively Charged Tricarboxylate, ACS Appl. Mater. Interfaces 11 (2019) 34497–34506.
[27] G. Xu, Z.A. Jarjes, V. Desprez, P.A. Kilmartin, J. Travas-Sejdic, Sensitive, selective, disposable electrochemical dopamine sensor based on PEDOT-modified laser scribed graphene, Biosens. Bioelectron. 107 (2018) 184–191.
[28] K. Promsuwan, L. Meng, P. Suklim, W. Limbut, P. Thavarungkul, P. Kanatharana, W.C. Mak, Bio-PEDOT: Modulating Carboxyl Moieties in Poly (3,4-ethylenedioxythiophene) for Enzyme-Coupled Bioelectronic Interfaces, ACS Appl. Mater. Interfaces 12 (2020) 39841–39849.
[29] N.F. Atta, A. Galal, R.A. Ahmed, Poly(3,4-ethylene-dioxythiophene) electrode for the selective determination of dopamine in presence of sodium dodecyl sulfate, Bioelectrochemistry 80 (2011) 132–141.
[30] A. Balamurugan, S.-M. Chen, Poly(3,4-ethylenedioxythiophene-co-(5-amino-2-naphthalenesulfonic acid)) (PEDOT-PANS) film modified glassy carbon electrode for selective detection of dopamine in the presence of ascorbic acid and uric acid, Anal. Chim. Acta 596 (2007) 92–98.
[31] R.F. Vreeland, C.W. Atcherley, W.S. Russell, J.Y. Xie, D. Lu, N.D. Laude, F. Porreca, M.L. Heien, Biocompatible PEDOT: Nafion Composite Electrode Coatings for Selective Detection of Neurotransmitters in Vivo, Anal. Chem. 87 (2015) 2600–2607.
[32] I. Gualandi, D. Tonelli, F. Mariani, E. Scavetta, M. Marzocchi, B. Fraboni, Selective detection of dopamine with an all PEDOT:PSS Organic Electrochemical Transistor, Sci. Rep. 6 (2016) 35419.
[33] J.M. George, A. Antony, B. Mathew, Metal oxide nanoparticles in electrochemical sensing and biosensing: a review, Microchim. Acta 185 (2018) 358.
[34] A. Cartwright, K. Jackson, C. Morgan, A. Anderson, D.W. Britt, A Review of Metal and Metal-Oxide Nanoparticle Coating Technologies to Inhibit Agglomeration and Increase Bioactivity for Agricultural Applications, Agronomy 10 (2020) 1018.
[35] J. Zhang, W. Chu, J. Jiang, X.S. Zhao, Synthesis, characterization and capacitive performance of hydrous manganese dioxide nanostructures, Nanotechnology 22 (2011) 125703.
[36] C.X. Guo, M. Wang, T. Chen, X.W. Lou, C.M. Li, A Hierarchically Nanostructured Composite of MnO_2/Conjugated Polymer/Graphene for High-Performance Lithium Ion Batteries, Adv. Energy Mater. 1 (2011) 736–741.
[37] J. Li, H. Shen, S. Yu, G. Zhang, C. Ren, X. Hu, Z. Yang, Synthesis of a manganese dioxide nanorod-anchored graphene oxide composite for highly sensitive electrochemical sensing of dopamine, Analyst 145 (2020) 3283–3288.
[38] R. Liu, J. Duay, S.B. Lee, Redox Exchange Induced MnO_2 Nanoparticle Enrichment in Poly(3,4-ethylenedioxythiophene) Nanowires for Electrochemical Energy Storage, ACS Nano 4 (2010) 4299–4307.
[39] Y. Wang, L. Wang, Q. Zhuang, A ratiometric electrochemical sensor for dopamine detection based on hierarchical manganese dioxide nanoflower/multiwalled carbon nanotube nanocomposite modified glassy carbon electrode, J. Alloy. Compd. 802 (2019) 326–334.
[40] K. Promsuwan, P. Kanatharana, P. Thavarungkul, W. Limbut, Subnanomolar detection of promethazine abuse using a gold nanoparticle-graphene nanoplatelet-modified electrode, Microchim. Acta 187 (2020) 646.
[41] K. Promsuwan, J. Thongtawat, W. Limbut, Porous palladium-poly(3,4-ethylenedioxythiophene)–coated carbon microspheres/graphene nanoplatelet–modified electrode for flow-based-amperometric hydrazine sensor, Microchim. Acta 187 (2020) 539.
[42] W.S. Hummers, R.E. Offeman, Preparation of Graphitic Oxide, J. Am. Chem. Soc. 80 (1958). 1339–1339.
[43] Z. Wang, X. Zhou, J. Zhang, F. Boey, H. Zhang, Direct Electrochemical Reduction of Single-Layer Graphene Oxide and Subsequent Functionalization with Glucose Oxidase, J. Phys. Chem. C 113 (2009) 14071–14075.
[44] S. Chen, J. Zhu, X. Wu, Q. Han, X. Wang, Graphene Oxide−MnO_2 Nanocomposites for Supercapacitors, ACS Nano 4 (2010) 2822–2830.
[45] T.K. Tam, M. Pita, M. Motornov, I. Tokarev, S. Minko, E. Katz, Electrochemical Nanotransistor from Mixed-Polymer Brushes, Adv. Mater. 22 (2010) 1863–1866.
[46] T.K. Tam, M. Pita, M. Motornov, I. Tokarev, S. Minko, E. Katz, Modified Electrodes with Switchable Selectivity for Cationic and Anionic Redox Species, Electroanalysis 22 (2010) 35–40.
[47] J.R. Sempionatto, M. Gamella, N. Guz, J.M. Pingarrón, V.A. Pedrosa, S. Minko, E. Katz, Electrochemically Stimulated DNA Release from a Polymer-Brush Modified Electrode, Electroanalysis 27 (2015) 2171–2179.
[48] C. Liu, R. Ding, F. Xie, Facile Synthesis of Manganese Dioxide Nanoparticles for Efficient Removal of Aqueous As(III), J. Chem. Eng. Data 65 (2020) 3988–3997.
[49] T.K. Tam, M. Pita, O. Trotsenko, M. Motornov, I. Tokarev, J. Halámek, S. Minko, E. Katz, Reversible "Closing" of an Electrode Interface Functionalized with a Polymer Brush by an Electrochemical Signal, Langmuir 26 (2010) 4506–4513.
[50] Y.-R. Kim, S. Bong, Y.-J. Kang, Y. Yang, R.K. Mahajan, J.S. Kim, H. Kim, Electrochemical detection of dopamine in the presence of ascorbic acid using graphene modified electrodes, Biosens. Bioelectron. 25 (2010) 2366–2369.
[51] V.S. Vasantha, S.-M. Chen, Electrocatalysis and simultaneous detection of dopamine and ascorbic acid using poly(3,4-ethylenedioxy)thiophene film modified electrodes, J. Electroanal. Chem. 592 (2006) 77–87.
[52] Z. Galus, Fundamentals of Electrochemical Analysis, 1976
[53] N.F. Atta, A. Galal, S.M. Ali, D.M. El-Said, Improved host–guest electrochemical sensing of dopamine in the presence of ascorbic and uric acids in a β-cyclodextrin/Nafion®/polymer nanocomposite, Anal. Methods 6 (2014) 5962–5971.
[54] G. Sheng, G. Xu, S. Xu, S. Wang, X. Luo, Cost-effective preparation and sensing application of conducting polymer PEDOT/ionic liquid nanocomposite with excellent electrochemical properties, RSC Adv. 5 (2015) 20741–20746.
[55] G. Xu, B. Li, X.T. Cui, L. Ling, X. Luo, Electrodeposited conducting polymer PEDOT doped with pure carbon nanotubes for the detection of dopamine in the presence of ascorbic acid, Sens. Actuators, B 188 (2013) 405–410.
[56] S. Harish, J. Mathiyarasu, K.L.N. Phani, V. Yegnaraman, PEDOT/Palladium composite material: synthesis, characterization and application to simultaneous determination of dopamine and uric acid, J. Appl. Electrochem. 38 (2008) 1583–1588.